# Intra-pulse Modulation Recognition of LPI Radar Signals Based on Improved MobileNet

*Jiaxin WU [1], Xudong WANG [1], Ye ZHOU [2], Binbin CHEN [1], Wuhang LI [1], Li ZHANG [1]*

[1] Dept. of the Key Laboratory of Radar Imaging and Microwave Photonics of the Ministry of Education, Nanjing University of Aeronautics and Astronautics, 29 Yudao Street, 210016 Nanjing, China
[2] Dept. of Civil Aircraft Center, Leihua Electronic Technology Research Institute, Aviation Industry Corporation of China (AVIC), 607 Shanshui East Road, 214063 Wuxi, China

{wwujiaxin, xudong}@nuaa.edu.cn, zhouy049@avic.com, cbb_220475@nuaa.edu.cn, li_wuhang@163.com, 1819871137@qq.com

Submitted April 10, 2025 / Accepted July 7, 2025 / Online first July 21, 2025

**Abstract.** *Addressing the challenge of feature extraction for Low Probability of Intercept (LPI) radar signals under low signal-to-noise ratio conditions, this study introduces a new method for intra-pulse modulation recognition of LPI radar signals based on an enhanced MobileNet architecture. Initially, a Time-Frequency Image (TFI) preprocessing technique suitable for LPI radar signals is proposed, which significantly improves the recognition accuracy of subsequent networks for intra-pulse modulation of LPI radar signals. Subsequently, the MobileNet network is modified by integrating Hybrid Dilation Convolution (HDC) and Efficient Channel Attention (ECA) modules, resulting in the development of an improved MobileNet. This enhanced network expands the receptive field of feature maps and improves the network's ability to capture channel and positional information. Additionally, a label smoothing strategy is utilized to optimize the network training process, reducing overfitting and enhancing sample clustering performance. Simulation experiments indicate that this method not only yields a high recognition accuracy rate but also outperforms existing comparative networks with fewer parameters.*

## Keywords

Low Probability of Intercept (LPI) radar signals, intra-pulse modulation recognition, Time-Frequency Analysis (TFA) technology, attention mechanism, lightweight convolutional neural network

## 1. Introduction

With the rapid development of electronic countermeasure technologies, the widespread application of Low Probability of Intercept (LPI) techniques has intensified competition between jamming and anti-jamming, leading to the emergence of various complex modulation types of LPI radar signals [1]. The low probability of intercept of these signals poses significant challenges for signal modulation recognition. In complex electromagnetic environments, the modulation recognition of LPI radar signals has become a crucial step from radar interception to information acquisition, serving as a core technology in radar reconnaissance and jamming. It is also a key issue that urgently needs to be addressed [2].

Traditional LPI radar signal recognition technologies based on pulse description words have failed to meet the demands of modern battlefield scenarios, prompting researchers to turn their focus to the exploration of the intra-pulse characteristics of LPI radar signals [3]. In recent years, with the significant advancement of deep learning in fields such as machine vision and natural language processing, the application of deep neural networks for the automatic recognition of LPI radar signal modulation schemes has become a research hotspot [4–7]. Literature [8] proposes a structure that combines Convolutional Neural Networks (CNN) with Long Short-Term Memory (LSTM) networks, where the CNN extracts spatial features and the LSTM captures temporal features, allowing for the simultaneous utilization of spatiotemporal information. Simulation results show that at a Signal-to-Noise Ratio (SNR) of –4 dB, the recognition accuracy for 8 types of LPI radar signals can reach 95.62%. Despite the high performance of this method, the CNN requires a large number of convolution, pooling, and matrix operations, leading to high computational complexity. Literature [9] introduces an LPI-Net-based deep convolutional neural network method for LPI radar waveform recognition, which, combined with the Choi-Williams Distribution (CWD) technique, achieves an accuracy rate exceeding 98% at 0 dB SNR. However, this method experiences a more severe interference from noise at low SNRs, which degrades its feature extraction capability and results in lower accuracy. Literature [10] proposes a CNN detection algorithm for four typical LPI radar signals, constructing detection models suitable for different modulation methods, parameters, and SNRs, and demonstrating good detection performance at low SNRs. Nevertheless, the performance of this algo-

DOI: 10.13164/re.2025.0461

rithm is dependent on the quality and quantity of the training data, while the limited variety of LPI radar signals results in limited generalization ability.

Despite the progress made by literatures [8–10] in enhancing the recognition capabilities of LPI radar signals, there remains a shortfall in the rapid identification of low-detectability LPI radar signals with similar features under low SNR environments. Addressing this issue, this study proposes an improved MobileNet-based method for intra-pulse modulation recognition of LPI radar signals. The main contributions are as follows:

- A TFI enhancement method is proposed, which effectively improves the accuracy of intra-pulse modulation recognition of LPI radar signals from the perspective of signal preprocessing.
- An efficient lightweight network is proposed, based on MobileNetV2 and incorporating Hybrid Dilated Convolution (HDC) and Efficient Channel Attention (ECA) modules, to construct the Dilated ECA-MobileNet (DEMNet). This expands the receptive field of the feature maps and enhances the network's ability to capture channel and positional information.
- To enhance the generalization capability of the network, a label smoothing strategy is introduced to avoid overfitting, thereby improving the accuracy and robustness of the model in recognizing unknown intra-pulse modulation types of LPI radar signals.

This paper is organized as follows: The second part elaborates on the innovative methods for establishing the signal model and the DEMNet model; the third part presents the experimental design and result analysis; and the fourth part summarizes the contributions of this paper.

# 2. Signal Model Establishment

## 2.1 LPI Radar Signal

LPI radar signals are specially designed radar signals aimed at reducing the likelihood of detection and interception by enemy electronic support measures systems while performing radar detection tasks. The general mathematical expression of an LPI radar signal is:

$$x(t) = A \cdot \mathrm{rect}(\frac{t}{T}) \cdot \exp(\mathrm{j}(2\pi f_c t + \varphi(t) + \varphi_0)), \quad (1)$$

$$\mathrm{rect}(\frac{t}{T}) = \begin{cases} 1, |t/T| \leqslant 1/2 \\ 0, |t/T| > 1/2 \end{cases} \quad (2)$$

where $A$ is the amplitude of the signal, $\mathrm{rect}(\cdot)$ is the gate function, $T$ is the pulse width of the signal, $f_c$ is the carrier frequency, $\varphi_0$ is the initial phase of the signal, and $\varphi(t)$ is the phase function with respect to time, which determines the modulation pattern of the signal.

## 2.2 Time-Frequency Feature Image Enhancement Processing

In the recognition process, the algorithm utilizes Time-Frequency Analysis (TFA) technology, transforming one-dimensional time-domain signals into two-dimensional time-frequency distribution maps, which is particularly critical [11]. Commonly used time-frequency analysis methods include Short Time Fourier Transform (STFT) [12], Wigner-Ville Distribution (WVD) [13], and Chirp-Wigner Distribution (CWD) [14]. Among them, WVD has excellent time-frequency resolution capabilities but suffers from the problem of cross-terms [15], [16]. This limitation has stimulated the development of techniques to suppress cross-terms, including CWD and Smoothed Pseudo Wigner-Ville Distribution (SPWVD). SPWVD is obtained by convolving WVD with a smoothing function and has good cross-term cancellation effects and time-frequency clustering features, leading to its widespread application in practical engineering [17]. The expression for SPWVD is as follows:

$$G(t,\omega) = \int_{-\infty}^{+\infty} g(u-t) \int_{-\infty}^{+\infty} h(\tau) x(t+\frac{\tau}{2}) x^*(t-\frac{\tau}{2}) \mathrm{e}^{-\mathrm{j}\omega\tau} \mathrm{d}\tau \mathrm{d}u \, . \quad (3)$$

In the expression, $g(u)$ and $h(\tau)$ represent the window functions in the time domain and frequency domain, respectively.

Although SPWVD can suppress some cross-terms, there is still noise and redundant information in the time-frequency image, making image enhancement preprocessing necessary, which involves grayscaling, Wiener filtering for noise reduction, principal component extraction, and adaptive cropping. This process is shown in Fig. 1.

Grayscale conversion removes the interference of color information while retaining the texture and structure of the image. Wiener filtering effectively adjusts the filter parameters based on the statistical characteristics of the input signal to minimize the mean square error of the output signal [18]. Principal component extraction is used to identify effective areas in the time-frequency image, with threshold detection determining the signal's start and end positions and extracting key features to eliminate redundant information. Adaptive cropping adjusts the height and width of the cropped time-frequency image to 224 × 224 using bilinear interpolation based on the input SNR parameters, thereby preserving more effective information and reducing noise.

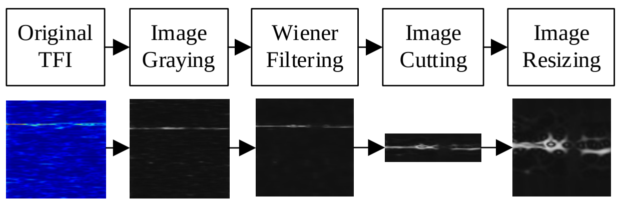


**Fig. 1.** TFI enhancement preprocessing flowchart (BPSK signal, SNR = −10 dB).

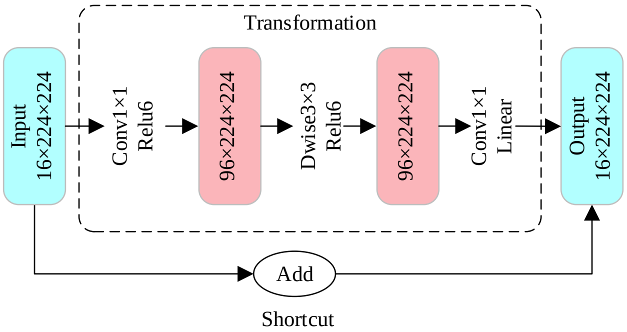


**Fig. 2.** Inverted residual network structure of MobileNetV2.

The signal preprocessing in this study first applies SPWVD time-frequency analysis to the input raw signals to obtain a series of time-frequency feature maps. Subsequently, these time-frequency feature maps undergo enhancement processing to enhance the recognizability of the features. This process ultimately completes the preprocessing of the signals.

# 3. Feature Extraction and Recognition Classification

## 3.1 Backbone Lightweight Network MobileNetV2

MobileNetV2, as a lightweight convolutional neural network, achieves a reduction in model size while maintaining better accuracy compared to MobileNetV1 [19]. The core of the MobileNetV2 architecture is the inverted residual structure, which combines depthwise separable convolution, residual connections, and Rectified Linear Unit (ReLU) activation functions [20]. As shown in Fig. 2, assuming an input feature map size of 16 × 224 × 224, the Inverted Residual Structure first increases the feature channels from 16 to 96 via the expansion layer to capture more information in high-dimensional space. Then, a 3 × 3 depthwise separable convolution is used to extract features and improve computational efficiency. Subsequently, the projection layer reduces the number of feature channels back to 16 to shrink the network size.

Unlike traditional residual structures, this module first expands the low-dimensional input to high-dimensional space, performs lightweight deep convolution, and then projects the features back to low dimensions via a linear bottleneck. The structure of MobileNetV2 significantly reduces model parameters and computational requirements while maintaining high accuracy, making it highly suitable for deployment on resource-constrained devices.

## 3.2 Hybrid Dilated Convolution

The core of dilated convolution is the dilation rate, which represents how much the original convolution kernel is expanded. The calculation method for the size of the expanded convolution kernel is as follows:

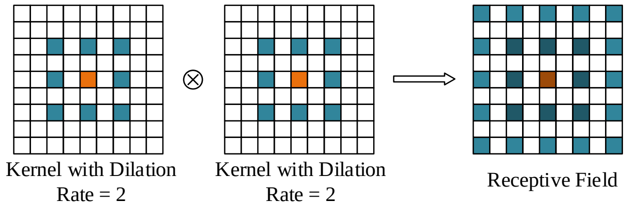


**Fig. 3.** Stacking effect of traditional dilated convolution kernels.

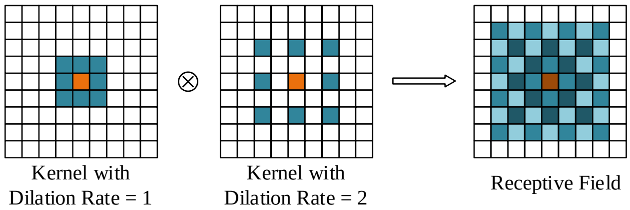


**Fig. 4.** Stacking effect of HDC kernels.

$$k_{\text{expanded}} = r \times (k-1) + 1. \tag{4}$$

In the formula, $k_{\text{expanded}}$ is the size of the dilated convolution kernel; $r$ is the dilation rate; and $k$ is the size of the original convolution kernel. However, stacking multiple dilated convolutions with the same dilation rate results in some pixels not being involved in the computation, leading to a significant loss of feature information and negatively impacting the final model's performance, as illustrated in Fig. 3.

Therefore, HDC is introduced with the goal of ensuring that the square receptive field is completely covered through a series of convolution operations, with no gaps or missing edges [21]. One principle of HDC is that the dilation rate must satisfy the corresponding formula and constraints. The maximum distance between two non-zero pixels is defined as:

$$M_i = \max[\, M_{i+1} - 2r_i, M_{i+1} - 2(\, M_{i+1} - r_i \,),\; r_i \,]. \tag{5}$$

In the formula, $M_i$ represents the maximum dilation rate that can be used at the $i^{\text{th}}$ layer; $r_i$ denotes the dilation rate at the $i^{\text{th}}$ layer. The constraint is $M_i \leq k$, and $k$ is the size of the convolution kernel. HDC also requires that the dilation rates of dilated convolutions must not have a common divisor greater than 1, in order to reduce the information loss caused by the gaps, as shown in Fig. 4.

## 3.3 Efficient Channel Attention Module

This study adopts the ECA attention mechanism, which is characterized by significantly reducing model complexity while maintaining performance [22]. The implementation of ECA is shown in Fig. 5. The input feature map has dimensions $H \times W \times C$, where $H$ denotes the height, $W$ the width, and $C$ the number of channels. Firstly, a global average pooling (GAP) is applied to compress the input from $H \times W \times C$ to $1 \times 1 \times C$ by averaging over the

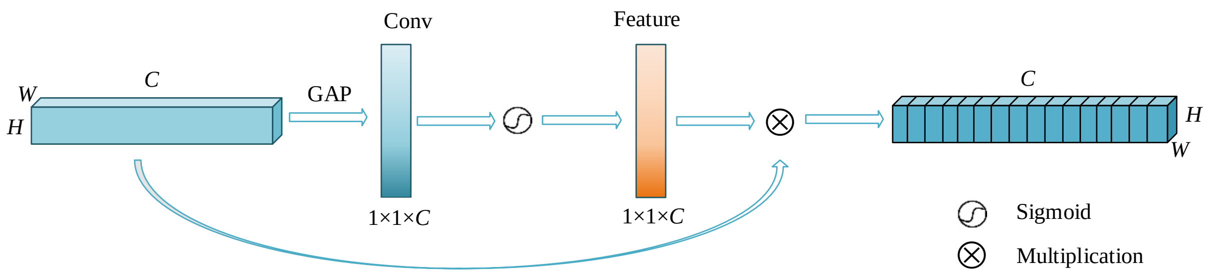


**Fig. 5.** Structure of the ECA attention mechanism.

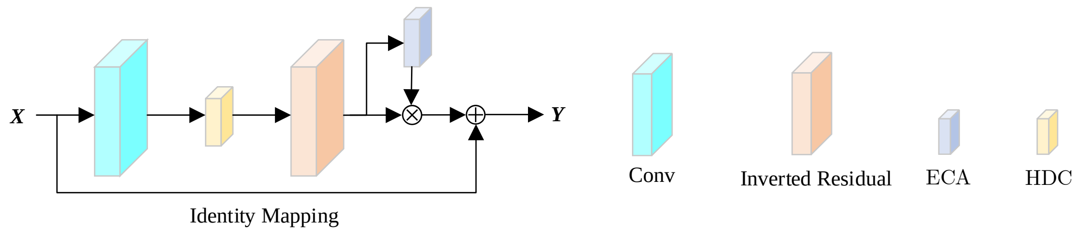


**Fig. 6.** DEM unit structure.

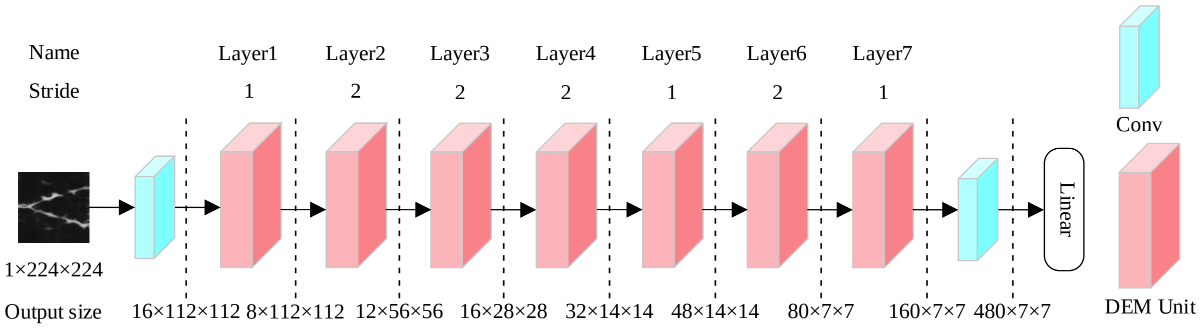


**Fig. 7.** Overall structure of DEMNet.

spatial dimensions ($H$ and $W$). Then, a convolution operation is used to process the GAP results to capture the interaction between local channels. After convolution, the Sigmoid function is used to compress the results into the [0,1] range, obtaining a weight vector for each channel. Finally, the weight vector is multiplied with the original feature map channel by channel, resulting in a weighted feature map, thus implementing the channel attention mechanism [23]. To enhance model performance and capture channel relationships and positional information, the ECA attention module is embedded within the residual structure.

## 3.4 DEMNet Network

Considering the characteristics of LPI radar signal time-frequency images, the goal is to minimize the network's parameters and computational complexity while ensuring a high recognition rate. Based on MobileNetV2 and incorporating HDC and ECA, a Dilated ECA-MobileNet Unit (DEM Unit) is designed, which is suitable for the recognition task of 12 types of LPI radar signals. Figure 6 shows the core structure of the DEM Unit. Each convolution operation consists of a convolutional layer, batch normalization (BN), and ReLU activation.

The DEMNet network is constructed by stacking and integrating multiple DEM Unit structures. The overall architecture of this network is depicted in Fig. 7. First, the input is the preprocessed time-frequency image with dimensions of $1 \times 224 \times 224$. It passes through a convolution layer, which serves to perform preliminary feature extraction on the input image. Next, a series of DEM Unit structures are applied to reduce the number of parameters and improve computational efficiency. After all the DEM Units are stacked, the network includes a final convolution layer to further adjust the number of channels in the feature map. Finally, the network outputs unnormalized scores through a linear transformation layer, which are then converted into a probability distribution via the softmax function.

In summary, by introducing attention mechanisms and hybrid dilated convolutions between the inverted residual structures, the network is able to learn the prominent features of images more effectively, achieving excellent performance in various visual tasks.

## 3.5 Label Smooth Cross Entropy Loss Function

In deep learning multi-classification tasks, the Cross-Entropy Loss ($L_{CE}$) is the standard method for measuring the discrepancy between predicted probabilities and true labels. Traditional $L_{\mathrm{CE}}$ uses the true labels directly, whereas the Label Smooth Cross Entropy Loss ($L_{\mathrm{LSCE}}$) employs smoothed labels. This smoothing is achieved by multiplying the true labels by a number less than 1, the label smoothing coefficient $\alpha_{\mathrm{LS}}$, and distributing the remainder evenly across the other classes. This approach prevents the model from being overconfident and enhances the model's generalization capability. The $L_{\mathrm{LSCE}}$ function is as follows [24]:

$$\bar{y}_n^{(m)} = (1-\alpha_{\mathrm{LS}})y_n^{(m)} + \frac{(1-y_n^{(m)})\alpha_{\mathrm{LS}}}{N_{\mathrm{class}}-1}, \quad (6)$$

$$L_{\mathrm{LSCE}} = -\frac{1}{N_{\mathrm{batch}}}\sum_{m=1}^{N_{\mathrm{batch}}}\sum_{n=1}^{N_{\mathrm{class}}} \bar{y}_n^{(m)} \log(p_n^{(m)}). \quad (7)$$

In the formula, $\bar{y}_n^{(m)}$ represents the true labels of $y_n^{(m)}$ after label smoothing, $p_n^{(m)}$ indicates the normalized predicted probability vector for sample. This study introduces $\alpha_{\mathrm{LS}}$ into the $L_{\mathrm{CE}}$ function to construct the $L_{\mathrm{LSCE}}$ function, in order to avoid overfitting.

# 4. Experimental Analysis

In the simulation experiment, 12 typical LPI radar intra-pulse modulation signals are simulated, including Binary Phase Shift Keying (BPSK), Frequency-Encoded Signals (Costas), Linear Frequency Modulated (LFM) signals, Non-Linear Frequency Modulated (NLFM) signals, Polyphase Codes (P1, P2, P3, P4), and Multi-Time Codes (T1, T2, T3, T4), making a total of 12 different signals for simulation. The parameters of these signals are detailed in Tab. 1. Here, the symbol $U()$ indicates that the parameter is uniformly randomly selected within a given range; [ ] indicates that the parameter can take any integer value within the range; and { } indicates that the parameter can only take specific discrete values. All the parameters are randomly selected within their respective value ranges. To preserve the time-frequency distribution characteristics of the signals, the signal sampling rate $f_s$ is normalized. The training set is generated within a SNR range of −8 dB to 8 dB, with a step size of 2 dB, resulting in a total of 27,648 time-frequency images (256 signals/class × 12 classes × 9 SNR steps). The test set is generated within an SNR range of −10 dB to 10 dB, with a step size of 2 dB, resulting in a total of 11,880 time-frequency images (90 signals/class × 12 classes × 11 SNR steps). For convenient referencing, the time-frequency image dataset without enhancement processing is named TFA-Original, and the dataset with enhancement processing is named TFA-IE.

| Signal type | Parameter | Symbol | Value range |
|---|---|---|---|
| BPSK | Carrier frequency | $f_c$ | $U(1/10,1/3)\cdot f_s$ |
| | Barker code length | $N_{\mathrm{code}}$ | $\{7,11,13\}$ |
| Costas | Hopping sequence | $N_s$ | $\{3,4,5,6\}$ |
| | Fundamental frequency | $f_{\min}$ | $U(1/24,1/20)\cdot f_s$ |
| LFM NLFM | Starting frequency | $f_0$ | $U(1/10,1/3)\cdot f_s$ |
| | Bandwidth | $B$ | $U(1/10,1/5)\cdot f_s$ |
| P1, P2 | Carrier frequency | $f_c$ | $U(1/10,1/3)\cdot f_s$ |
| | Number of frequency steps | $M$ | $[8,12]$, $M$ of P2 is even |
| | Cycles per phase code | cpp | $[2,5]$ |
| P3, P4 | Carrier frequency | $f_c$ | $U(1/10,1/3)\cdot f_s$ |
| | Number of frequency steps | $M$ | $\{36,64,81,100\}$ |
| | Cycles per phase code | cpp | $[2,5]$ |
| T1, T2 | Carrier frequency | $f_c$ | $U(1/10,1/3)\cdot f_s$ |
| | Number of segments | $N_k$ | $[4,6]$ |
| T3, T4 | Carrier frequency | $f_c$ | $U(1/10,1/3)\cdot f_s$ |
| | Number of segments | $N_k$ | $[4,6]$ |
| | Bandwidth | $B$ | $U(1/20,1/8)\cdot f_s$ |

**Tab. 1.** Signal simulation parameters.

## 4.1 Comparison of Recognition Accuracy among Different Networks

To investigate the impact of using different networks on the recognition performance of LPI radar signals, the SPWVD-IE dataset was used to train five networks: MobileNetV2, ResNet18 [25], ResNet34 [26], ResNet50 [27], and GoogLeNet [28]. The recognition accuracies of these five networks for 12 types of LPI radar signals under different SNRs are shown in Fig. 8. The graph shows MobileNetV2 has a higher accuracy rate than GoogLeNet, reaching 97.22% at –10 dB, compared to lower rates for ResNet18, ResNet34, and ResNet50. MobileNetV2 excels in low SNR conditions, suggesting it is better at recognizing signals with low SNRs.

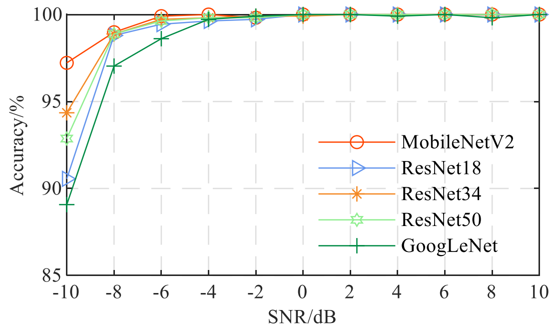


**Fig. 8.** Comparison of recognition accuracy for different networks.

| Network | Flops (M) | Params (M) |
|---|---|---|
| MobileNetV2 | 238.43 | 1.70 |
| ResNet18 | 1750.00 | 11.18 |
| ResNet34 | 3600.00 | 21.28 |
| ResNet50 | 4050.00 | 23.53 |
| GoogLeNet | 2000.00 | 0.91 |

**Tab. 2.** Comparison of floating point operations and number of parameters for different networks.

To evaluate the computational complexity, storage requirements and practical performance of different networks, the floating point operations (Flops) and number of parameters (Params) were used as evaluation metrics. The experimental results are shown in Tab. 2. Flops, measured in millions (M), are used to assess the computational complexity of the network, while the number of parameters, also measured in millions (M), is used to evaluate the storage requirements of the network.

Based on the floating point operations and number of parameters, MobileNetV2 has relatively low computational complexity and parameter count, making it more practical in resource-constrained environments, which positions it as a lightweight network. Although GoogLeNet has a relatively low number of parameters, its floating point operations are higher, indicating that it requires more computational resources and storage space when handling complex tasks. When balancing accuracy and complexity, MobileNetV2 significantly reduces both parameters and Flops while achieving high accuracy.

## 4.2 Comparison of Different Time-Frequency Analysis Methods

In order to investigate the impact of different preprocessing methods on the network recognition performance of LPI radar signals, this section selects two time-frequency analysis techniques: SPWVD and STFT. Based on these two time-frequency analysis methods, corresponding image-enhanced datasets were constructed: SPWVD-IE and STFT-IE. By training DEMNet on these datasets, their performance in recognizing 12 types of LPI radar signals was evaluated. At an SNR of –8 dB, 90 time-frequency image samples were selected from the test set of each signal category from the four datasets to generate the corresponding confusion matrices, as shown in Fig. 9. The horizontal axis represents the true category proportion of the samples, while the vertical axis represents the predicted category proportion for the corresponding samples.

From Fig. 9, it is clear that compared to Fig. 9(a), Fig. 9(b) shows more significant confusion in P1, P3, and P4, indicating the effectiveness of time-frequency feature image enhancement for LPI radar signal recognition. When Fig. 9(a) and Fig. 9(c) are compared, the STFT-IE dataset shows more serious confusion in P4 and P1, demonstrating that among the two time-frequency analysis methods, SPWVD is more effective. Furthermore, a comparison of Fig. 9(a) and Fig. 9(d) further confirms the effectiveness of both image enhancement processing and SPWVD time-frequency analysis.

## 4.3 Comparison of Recognition Accuracy with Different Attention Mechanisms

To analyze the impact of the ECA module and Hybrid Dilated Convolution on the network's recognition perfor-

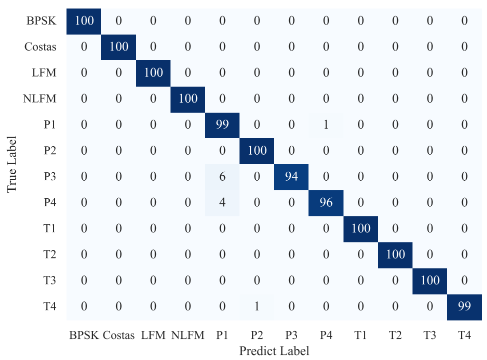


(a) SPWVD-IE confuse_matrix.

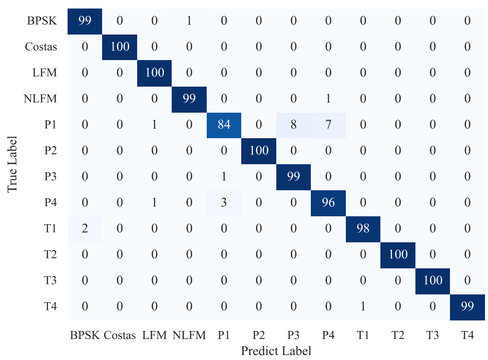


(b) SPWVD confuse_matrix.

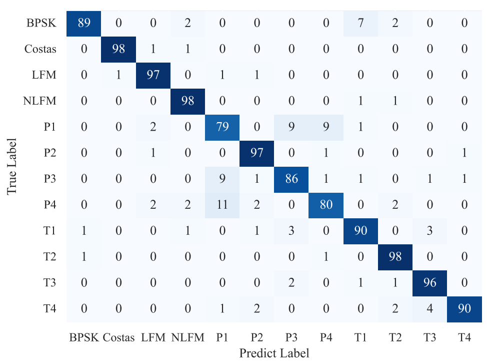


(c) STFT-IE confuse_matrix.

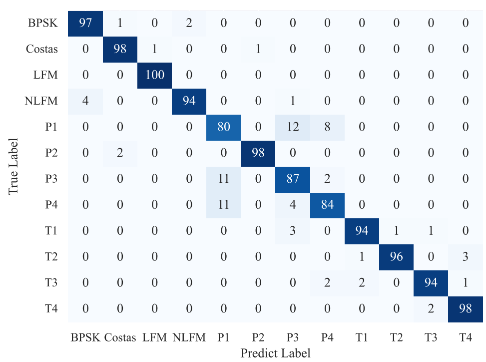


(d) STFT confuse_matrix.

**Fig. 9.** Comparison of confusion matrices.

mance, we first embedded different attention mechanisms—ECA, Coordinate Attention (CA), and Convolutional Block Attention Module (CBAM)—at the same positions within the Dilated MobileNetV2 (DMNet) that uses Hybrid Dilated Convolution. This resulted in the networks DEMNet, CA-DMNet, and CBAM-DMNet, respectively. Then, for the network with the best recognition performance, we removed the Hybrid Dilated Convolution, and obtained the EMNet network, which only incorporated the ECA attention mechanism. All four networks were trained and tested on the SPWVD-IE dataset, and the recognition results for these networks are shown in Fig. 10. Overall, DEMNet performed significantly better than the other networks under low SNR conditions, which demonstrates the effectiveness of the ECA attention mechanism and HDC.

To more intuitively showcase the contribution of the three attention mechanisms to the network's time-frequency feature extraction, Grad-CAM visualization was applied to show the feature extraction results for the 12 types of LPI radar signals processed by DEMNet, CA-DMNet, and CM-DMNet. Heatmaps of the attention mechanisms for recognizing LFM signals, NLFM signals, P3 signals, and P4 signals are shown in Fig. 11.

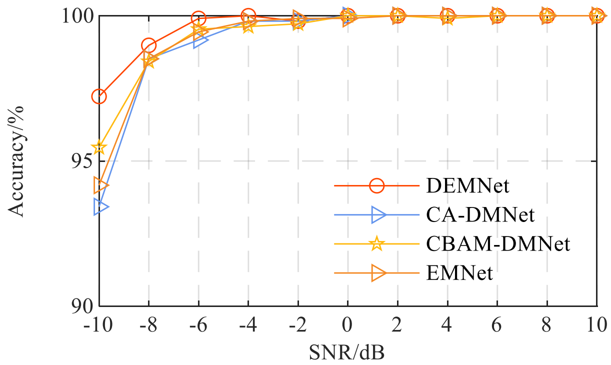


**Fig. 10.** Comparison of recognition accuracy with different attention mechanisms.

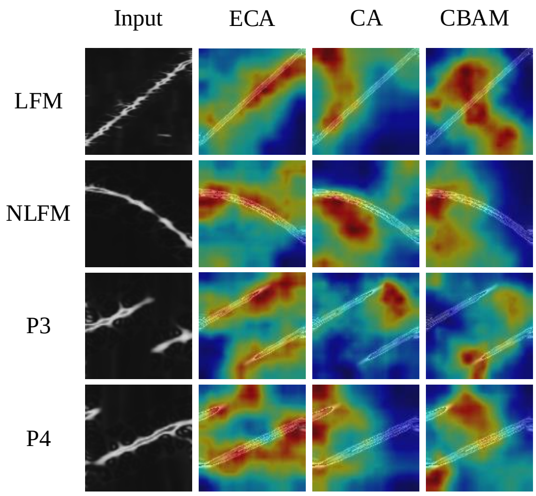


**Fig. 11.** Comparison of heatmaps with different attention mechanisms.

As shown in the figure, when the network recognizes the above test samples, they are susceptible to background noise, resulting in dispersed and incomplete attention areas. The ECA attention mechanism shows more prominent attention areas in the heatmaps for the four signals, particularly in the central area of the images, indicating that it can better recognize and emphasize these areas.

## 4.4 Analysis of the Effectiveness of Label Smoothing Loss

To validate the effect of label smoothing loss on the network's recognition performance, we attempted to optimize the network proposed in this study using two loss functions during the DEMNet network training process, namely the $L_{\mathrm{CE}}$ and $L_{\mathrm{LSCE}}$ functions. Additionally, we conducted a sweep experiment on the selection of the label smoothing coefficient. During the two training processes, we maintained consistency in dataset partitioning, model, optimizer, and other factors, to directly compare the recognition performance differences brought about by different losses. From the SPWVD-IE test dataset, 90 samples were randomly selected from each class of signals. Under different loss functions, the t-Distributed Stochastic Neighbor Embedding (t-SNE) method was used to project the input samples and the features extracted by the network onto a two-dimensional plane, respectively. The resulting sample clustering effects are shown in Fig. 12.

Figure 12(a) represents the clustering diagram of the input samples, while Figure 12(b) and Figure 12(c) show the clustering diagrams of the features extracted by the network after dimensionality reduction under the $L_{\mathrm{CE}}$ and $L_{\mathrm{LSCE}}$ functions, respectively. From the figure, it can be observed that the different categories of input samples overlap, and the dispersion within each signal class is large. When the network is trained using only the Cross-Entropy Loss, individual samples of one signal class are mixed with signals of different classes. However, when label smoothing loss is introduced, the inter-class distances between different signals increase, and the intra-class signals exhibit better clustering. This indicates that label smoothing effectively increases the separation between different signals, thereby improving the network's recognition accuracy.

Figure 13 shows the results of the traversal experiment for the best value of the weight hyperparameter in the label smoothing loss function. During training, different values of $\alpha_{\mathrm{LS}}$ ranging from 0.1 to 0.95 were tested to observe their impact on the accuracy. As shown in Fig. 13, introducing the label smoothing coefficient $\alpha_{\mathrm{LS}}$ influences the network's signal recognition accuracy. The network achieved the highest recognition accuracy of 99.84% when $\alpha_{\mathrm{LS}}$ was set to 0.65. Therefore, the final experiment chose $\alpha_{\mathrm{LS}} = 0.65$ to achieve the optimal recognition performance of the network.

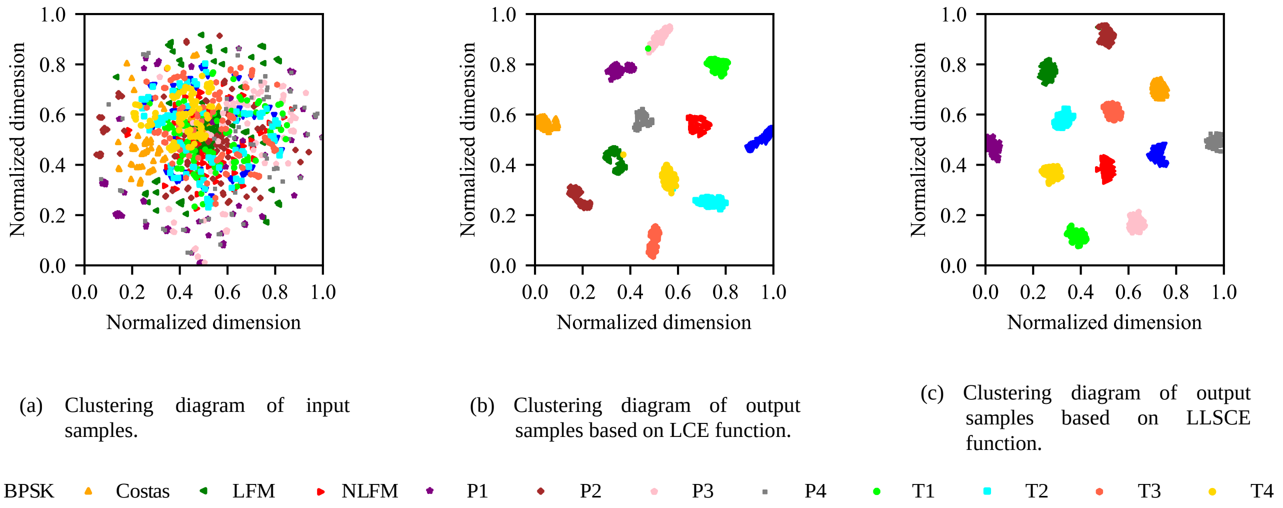


(a) Clustering diagram of input samples.

(b) Clustering diagram of output samples based on LCE function.

(c) Clustering diagram of output samples based on LLSCE function.

**Fig. 12.** Clustering diagrams of input samples and output samples after training with different loss functions.

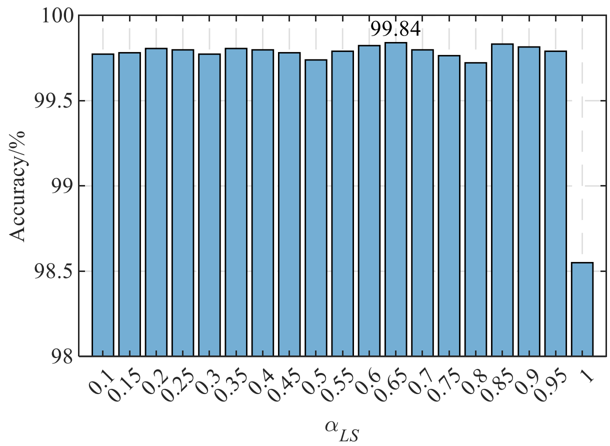


**Fig. 13.** Impact of the label smoothing coefficient on network recognition accuracy.

## 5. Conclusion

This study proposes an LPI radar signal intra-pulse modulation recognition method based on DEMNet. Three main improvements are made to enhance the LPI radar signal recognition technology. First, image enhancement preprocessing is used to reduce noise interference, remove redundant frequency bands. Second, hybrid dilated convolutions and an efficient channel attention module are introduced into MobileNetV2, further enhancing its ability to capture channel and positional information. Additionally, label smoothing strategy is applied to avoid overfitting, thereby improving the model's accuracy and robustness in recognizing unknown LPI radar signal intra-pulse modulation types. The experimental results show that, compared to existing methods, the recognition method proposed in this study not only yields a high recognition accuracy rate but also features fewer parameters and lower computational cost, thus meeting the design requirements for network lightweight and efficient training.

## Acknowledgments

This study was thankfully supported in part by the Civil Aircraft Project.

## References

[1] REN, F., QUAN, D., SHEN, L., et al. LPI radar signal recognition based on feature enhancement with deep metric learning. *Electronics*, 2023, vol. 12, no. 24, p. 1–16. DOI: 10.3390/electronics12244934

[2] LIU, Z., WANG, J., WU, T., et al. A method for LPI radar signals recognition based on complex convolutional neural network. *International Journal of Numerical Modelling: Electronic Networks, Devices and Fields*, 2023, vol. 37, no. 1, p. 1–13. DOI: 10.1002/jnm.3155

[3] MI, X., CHEN, X., LIU, Q., et al. Radar signals modulation recognition based on bispectrum feature processing. *Journal of Physics: Conference Series*, 2021, vol. 1971, no. 1, p. 1–11. DOI: 10.1088/1742-6596/1971/1/012099

[4] CHEN, B., WANG, X., ZHU, D., et al. LPI radar signals modulation recognition in complex multipath environment based on improved ResNeSt. *IEEE Transactions on Aerospace and Electronic Systems*, 2024, vol. 60, no. 6, p. 8887–8900. DOI: 10.1109/TAES.2024.3436634

[5] ZHANG, X., LIU, Y., YAN, X., et al. Frequency modulation recognition for radar signal based on Resnet-LSTM network. *Artificial Intelligence Technology Research*, 2024, vol. 2, no. 3, p. 100–102. DOI: 10.18686/aitr.v2i3.4426

[6] QUAN, D., TANG, Z., WANG, X., et al. LPI radar signal recognition based on dual-channel CNN and feature fusion. *Symmetry*, 2022, vol. 14, no. 3, p. 1–13. DOI: 10.3390/sym14030570

[7] WAN, C., SI, W., DENG, Z. Research on modulation recognition method of multi-component radar signals based on deep convolution neural network. *IET Radar, Sonar & Navigation*, 2023, vol. 17, no. 9, p. 1313–1326. DOI: 10.1049/rsn2.12421

[8] RUAN, G., WANG, Y., WANG, L., et al. Automatic recognition of radar signal types based on CNN-LSTM. *Telecommunications*

*and Radio Engineering*, 2020, vol. 79, no. 4, p. 305–321. DOI: 10.1615/TelecomRadEng.v79.i4.40

[9] JIANG, Y., YIN, Z., SONG, Y. Low probability of intercept radar signal detection algorithm based on convolution neural network (in Chinese). *Journal of Electronics and Information Technology*, 2022, vol. 44, no. 2, p. 718–725. DOI: 10.11999/JEIT210132

[10] HUYNH-THE, T., DOAN, V.-S., HUA, C.-H., et al. Accurate LPI radar waveform recognition with CWD-TFA for deep convolutional network. *IEEE Wireless Communications Letters*, 2021, vol. 10, no. 8, p. 1638–1642. DOI: 10.1109/LWC.2021.3075880

[11] DONG, N., JIANG, H., LIU, Y., et al. Intra-pulse modulation radar signal recognition using CNN with second-order STFT-based synchro squeezing transform. *Remote Sensing*, 2024, vol. 16, no. 14, p. 1–13. DOI: 10.3390/rs16142582

[12] ZHOU, Z., HUANG, G., CHEN, H., et al. Automatic radar waveform recognition based on deep convolutional denoising auto-encoders. *Circuits, Systems, and Signal Processing*, 2018, vol. 37, no. 9, p. 4034–4048. DOI: 10.1007/s00034-018-0757-0

[13] THOMAS, M., JACOB, R., LETHAKUMARY, B. Comparison of WVD based time-frequency distributions. In *2012 International Conference on Power, Signals, Controls and Computation.* Thrissur (India), 2012, p. 1–8. DOI: 10.1109/EPSCICON.2012.6175242

[14] SI, W., WAN, C., DENG, Z. An efficient deep convolutional neural network with features fusion for radar signal recognition. *Multimedia Tools and Applications*, 2023, vol. 82, no. 2, p. 2871 to 2885. DOI: 10.1007/s11042-022-13407-9

[15] CHEN, J., LI, B. The short-time Wigner–Ville distribution. *Signal Processing*, 2024, vol. 219, p. 1–13. DOI: 10.1016/j.sigpro.2024.109402

[16] SINGH, V. K., PACHORI, R. B. Sliding eigenvalue decomposition-based cross-term suppression in Wigner–Ville distribution. *Journal of Computational Electronics*, 2021, vol. 20, no. 6, p. 2245–2254. DOI: 10.1007/s10825-021-01781-w

[17] LIU, L., LI, X. Radar signal recognition based on triplet convolutional neural network. *EURASIP Journal on Advances in Signal Processing*, 2021, vol. 2021, no. 1, p. 1–16. DOI: 10.1186/s13634-021-00821-8

[18] HEPSIBA, D., JUSTIN, J. Enhancement of single channel speech quality and intelligibility in multiple noise conditions using Wiener filter and deep CNN. *Soft Computing*, 2022, vol. 26, no. 23, p. 13037–13047. DOI: 10.1007/s00500-021-06291-2

[19] SHAHI, T. B., SITAULA, C., NEUPANE, A., et al. Fruit classification using attention-based MobileNetV2 for industrial applications. *PloS one*, 2022, vol. 17, no. 2. DOI: 10.1371/journal.pone.0264586

[20] ZHAO, L., WANG, L., JIA, Y., et al. A lightweight deep neural network with higher accuracy. *Plos one*, 2022, vol. 17, no. 8. DOI: 10.1371/journal.pone.0271225

[21] BIAN, S., HE, X., XU, Z., et al. Hybrid dilated convolution with attention mechanisms for image denoising. *Electronics*, 2023, vol. 12, no. 18, p. 1–17. DOI: 10.3390/electronics12183770

[22] WANG, Q., WU, B., ZHU, P., et al. ECA-Net: Efficient channel attention for deep convolutional neural networks. In *Proceedings of the IEEE/CVF Conference on Computer Vision and Pattern Recognition.* Seattle (WA, USA), 2020, p. 11531–11539. DOI: 10.1109/CVPR42600.2020.01155

[23] WANG, Y., LI, R., WANG, Z., et al. E3D: An efficient 3D CNN for the recognition of dairy cow's basic motion behavior. *Computers and Electronics in Agriculture*, 2023, vol. 205, p. 1–12. DOI: 10.1016/j.compag.2022.107607

[24] SHAO, G., CHEN, Y., WEI, Y. Deep fusion for radar jamming signal classification based on CNN. *IEEE Access*, 2020, vol. 8, no. 1, p. 117236–117244. DOI: 10.1109/ACCESS.2020.3004188

[25] ZHANG, Y., PENG, L., MA, G, et al. Dynamic gesture recognition model based on millimeter-wave radar with ResNet-18 and LSTM. *Frontiers in Neurorobotics*, 2022, vol. 16, p. 1–9. DOI: 10.3389/fnbot.2022.903197

[26] SONG, Q., HUANG, S., ZHANG, Y., et al. Radar target classification using enhanced Doppler spectrograms with ResNet34CA in ubiquitous radar. *Remote Sensing*, 2024, vol. 16, no. 15, p. 1–24. DOI: 10.3390/rs16152860

[27] LIANG, J., LUO, Z., LIAO, R. Intra-pulse modulation recognition of radar signals based on efficient cross-scale aware network. *Sensors*, 2024, vol. 24, no. 16, p. 1–17. DOI: 10.3390/s24165344

[28] WANG, G., CHEN, S., HUANG, J., et al. Radar signal sorting and recognition based on transferred deep learning (in Chinese). *Computer Science and Application*, 2019, vol. 9, no. 9, p. 1761 to 1778. DOI: 10.12677/CSA.2019.99198

## About the Authors ...

**Jiaxin WU** was born in Quzhou, Zhejiang Province, China in 2001. She received a B.S. degree in Communication Engineering from Nanjing University of Science and Technology ZiJin College, Nanjing, China in 2023. She is currently pursuing an M.S. degree at the College of Electronic and Information Engineering, Nanjing University of Aeronautics and Astronautics (NUAA), Nanjing, China. Her current research interests include radar signal processing and machine learning.

**Xudong WANG** (corresponding author) was born in Huainan, Anhui Province, China in 1978. He received his B.S., M.S., and Ph.D. degrees in Communication Engineering from Nanjing University of Aeronautics and Astronautics (NUAA), Nanjing in 2001, 2004, and 2008, respectively. Currently, he is an Associate Professor at the College of Electronic and Information Engineering, Nanjing University of Aeronautics and Astronautics. His research interests include radar signal processing and FPGA hardware implementation.

**Ye ZHOU** was born in Wuxi, Jiangsu Province, China, in 1982. She received her B.S. and M.S. degrees from Nanjing University of Science and Technology. She is currently a Senior Engineer at the Civil Aircraft Center, LeiHua Electronic Technology Research Institute, Aviation Industry Corporation of China. Her research interests include radar signal processing.

**Binbin CHEN** was born in Wuhu, Anhui Province, China in 2000. He received his B.S. degree in Communication Engineering from Anhui Normal University in 2022. He is currently pursuing a Ph.D. degree through a combined master's and doctoral program at the College of Electronic and Information Engineering, NUAA, Nanjing, China. His current research interests include radar signal processing and machine learning.

**Wuhang LI** was born in Fuzhou, Fujian Province, China in 2002. He received his B.S. degree in Communication Engineering from Huaqiao University, Xiamen, China in 2024. He is currently pursuing an M.S. degree at the College of Electronic and Information Engineering, Nanjing University of Aeronautics and Astronautics (NUAA), Nanjing, China. His current research interests include radar signal processing and machine learning.

**Li ZHANG** was born in Dazhou City, Sichuan Province, China in 2001. She received her B.S. degree in Communication Engineering from Hohai University, Nanjing, China in 2024. She is currently pursuing an M.S. degree at the College of Electronic and Information Engineering, Nanjing University of Aeronautics and Astronautics (NUAA), Nanjing, China. Her current research interests include radar signal processing and machine learning.